Characterization of the formability limit by fracture in mode III of fracture mechanics of sheets

Pedro Nuno Clemente Leonardo

pedro.leonardo@tecnico.ulisboa.pt

Instituto Superior Técnico, Universidade de Lisboa, Lisboa, Portugal
November 2019

Abstract: This document is focused on the characterization of the fracture limits in sheet-bulk forming. The approach extends to crack opening in mode III (out-of-plane shearing), a digital image correlation-based methodology for determining the fracture forming limits in mode I (tension) and mode II (in-plane shearing). For this purpose, a sheet lengthwise compression test with different end constraints is developed and utilized to obtain the strain loading paths up to fracture in mode III, for the first time directly from sheets. Regarding the characterization of modes I and II of fracture mechanics, four types of conventional tests were used. The three fracture forming limits of sheet-bulk forming are first characterized in principal strain space and then transformed into the space of effective strain vs. stress triaxiality by using Hill's yield plasticity criterion. A new uncoupled ductile damage criterion is introduced and successfully implemented in the finite element computer program *i-form 3d* to predict the location where the out-of-plane shearing cracks are triggered.

Keywords: Sheet-Bulk Forming, Fracture Forming Limits, Mode III of Fracture Mechanics, Ductile Damage, Sheet Lengthwise Compression, Experimentation, Finite Element Method.

1. INTRODUCTION

In the last years there has been a growing demand for stamped products whose manufacturing processes fall under the category of what is nowadays referred to as 'sheet-bulk forming' [1] or 'plate forging' [2]. Sheet-bulk forming (SBF) combines plane stress loading conditions of sheet forming with three-dimensional stress loading conditions of bulk forming to shape local functional features such as solid bosses, teeth and ribs outside the plane of the sheets from which the stamped products are manufactured (Fig. 1a).

The primary goals of adding local functional features in stamped products is that savings can be made in the number of individual parts to be assembled, maintenance costs reduced and total weight improved. All this is achievable thanks to the following three main types of out-of-plane plastic flow that SBF can add to conventional sheet forming: (i) thickening, (ii) local thickening and (iii) injection (Fig. 1b and 1c).

Because the three above-mentioned types of plastic flow exploit the limits of process workability, efforts have been made to understand the physics underlying the typical defects that are likely to occur in SBF and to develop technical solutions to prevent their occurrence. Typical defects are schematically depicted in Fig. 1d and consist of buckling and/or folding of the sheet/side wall, free surface cracking and internal flaws that eventually lead to through-thickness cracking.

The physics underlying the occurrence and development of buckling and folding is well-understood because the collapse of plates and shells subjected to compression loading is governed by the theory of stability [3] and the kinematics of folding is governed by the mechanics of contact (or self-contact) between plastically deformable objects [4]. This means that both types of defects can be easily handled by finite element computations.
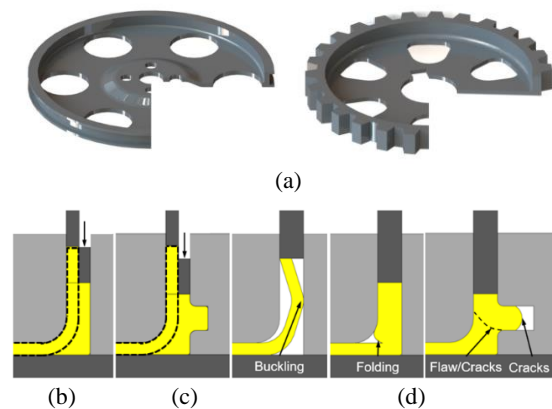

Fig. 1 - Material flow types in sheet-bulk forming: (a) Belt pulley and gear drum produced by sheet-bulk forming; (b) Schematic representation of thickening or local thickening in SBF; (c) Schematic representation of injection in SBF; (d) Illustration of the four different types of defects that are likely to occur in SBF.

Regarding the other two defects due to cracking, one can start by saying that the physical phenomena related to their occurrence and development are also relatively well-understood. Basic knowledge relies upon combination of concepts retrieved from plasticity theory, ductile damage mechanics and fracture mechanics, namely the fundamental crack opening modes by tension, in-plane shearing and out-of-plane-shearing, as proposed by Martins et al. [5].

However, this document raises a two-fold challenge that has never been addressed before. Firstly, how to characterize the fracture forming limits in principal strain space and in the space of effective strain vs. stress triaxiality for the three different crack opening modes that are likely to occur in SBF [6]. Secondly, whether the application of conventional uncoupled ductile damage criteria can predict the location and the amount of deformation after which cracks are triggered in SBF.

The first challenge can be overcome if one has access to sheets and rods (or, thick plates) of the same material with similar supplied conditions. Formability limits by fracture in sheet forming can be characterized using the well-known methods and procedures involving the following two main groups of tests [7]: (i) tensile, double notched tensile, bulge (circular and elliptical) and Nakajima tests to determine the fracture forming line (FFL) corresponding to crack opening mode I (by tension), (ii) shear tests with varying ligament sizes and staggered double notched tensile tests with different ligament sizes and inclination angles to determine the shear fracture forming line (SFFL) corresponding to crack opening mode II (by in-plane shearing) (Fig. 2a).
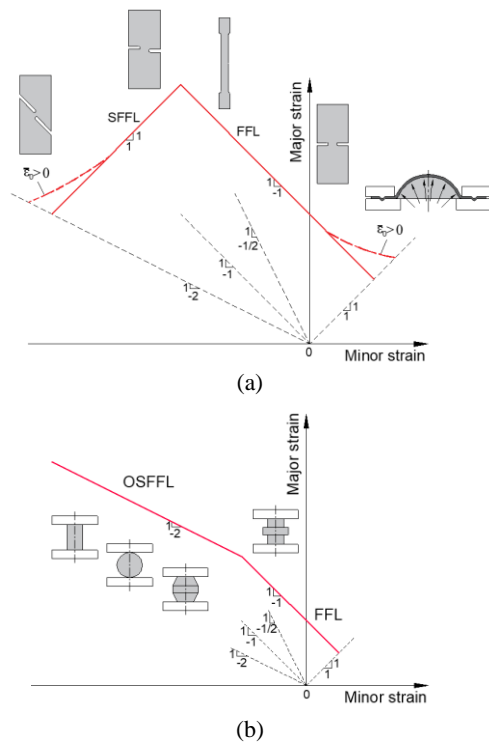

(a)

(b)

Fig. 2 - Schematic representation of the fracture forming limits in principal strain space for (a) sheet forming and (b) bulk forming. The inset drawings show some of the most commonly used test specimens.

On the other hand, if there are rods (or thick plates) of the same material with similar supplied conditions, the fracture forming lines of bulk forming can also be easily determined through compression tests performed on cylindrical, tapered and flanged specimens [8]. This allows determining the

out-of-plane fracture forming line (OSFFL) corresponding to crack opening mode III (by out-of-plane/through-thickness shearing), and to obtain additional fracture strains on the previously determined FFL associated to mode I [9] (Fig. 2b).

Under these circumstances, the first challenge arising from SBF is the necessity of characterizing the fracture forming limits corresponding to the three different crack opening modes in raw materials that are exclusively supplied as sheets.

Thus, the first objective of this document is to propose a methodology based on the utilization of digital image correlation and thickness measurements to determine the strain loading paths and the fracture strains for a set of tests capable of providing crack opening by tension, in-plane shear and out-of-plane shear. Special emphasis is given to a new formability test consisting on the lengthwise compression of a sheet between flat parallel platens with different end support conditions until cracking by out-of-plane (through-thickness, mode III) shearing. The fracture forming limits derived from this first objective are plotted in principal strain space and in the space of effective strain versus stress-triaxiality.

The second challenge arising from SBF that will also be addressed in this document is focused on the performance of simple uncoupled ductile damage criteria built upon weighted integrations of plastic strain [10]. For this purpose classical ductile damage criteria due to McClintock [11], often referred to as the Ayada damage criterion (after Ayada et al. [12]), Cockcroft-Latham [13] and shear based [5] will be tested against a new ductile damage criterion proposed to predict the location and the amount of deformation upon which cracks are triggered. The new proposed criterion is built upon the work of McClintock et al. [14] for modelling fracture in shear bands based on opening and growth of neighbouring voids.

2. EXPERIMENTATION

2.1. Mechanical Characterization

Mechanical characterization of the commercial AW7075-T651 aluminium sheets with 5 mm thickness that were utilized in the investigation was carried out by means of tensile and stack compression tests. The tensile tests were performed in accordance to ASTM standard E8/E8M-16 [15] and the specimens were machined out from the supplied sheets at 0, 45 and 90 degrees with respect to the rolling direction (RD) to evaluate the influence of anisotropy.

The stack compression test specimens were prepared by pilling-up three circular discs with 15 mm diameter and 5 mm thickness that were also machined out from the supplied sheets. The main purpose of the stack compression tests was to obtain the stress response for values of strain beyond plastic instability in tension because some fracture tests performed in this investigation reach high strains.

These tests were performed in accordance to ASTM standard E9-18 [16].

Both tensile and stack compression tests were carried out at room temperature and the resulting stress-strain curves are disclosed in Fig. 3.
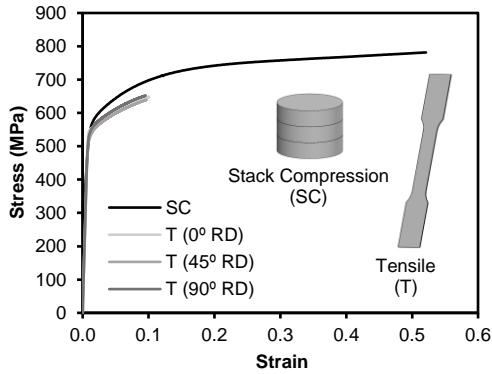

Fig. 3 - True stress-true strain curves of aluminium AW7075-T651 obtained from tensile (T) and stack compression (SC) tests.

Table 1 provides the modulus of elasticity E, the yield strength σ_Y, the ultimate tensile strength σ_{UTS}, the elongation at break A and the anisotropy coefficient r for the tensile tests performed with specimens cut out at 0, 45 and 90 degrees with respect to the rolling direction (RD). The average values included in Table 1 were determined as follows (where $\bar{x}$ denotes a mechanical property),

$$\bar{x} = \frac{x_0 + 2x_{45} + x_{90}}{4} \quad (1)$$

Table 1 - Mechanical properties of the aluminium AW7075-T651 sheets obtained from tensile tests.

	0º RD	45º RD	90º RD	Avg.
E (GPa)	73.30	71.18	71.24	71.72
σ_Y (MPa)	538.51	509.01	525.56	520.52
σ_{UTS} (MPa)	586.76	579.31	593.30	584.67
A (%)	15.94	14.08	14.09	14.55
r	0.533	0.672	0.774	0.663

The planar anisotropy Δr is calculated from the anisotropy coefficients r_i included in Table 1, as follows,

$$\Delta r = \frac{r_0 - 2r_{45} + r_{90}}{2} \cong -0.018 \quad (2)$$

The result obtained in (2) allows concluding that the mechanical behaviour of the AW7075-T651 aluminium sheets does not present significant variations with angle from the rolling direction. Moreover $\bar{r} = 0.663$ in Table 1 reveals that normal anisotropy is relevant and, therefore, should be taken into consideration.

2.2. Fracture tests

Table 2 presents a summary of the different tests that were used for determining the fracture forming lines corresponding to crack opening modes I, II and III. The tests are grouped in three different categories. Category I contains the tensile (T) and the double-notched tensile (DNT) tests that were utilized to determine the FFL corresponding to failure by crack opening mode I (by tension). Category II contains the shear (S) and the staggered double-notched tensile (SDNT) tests that were utilized to determine the SFFL corresponding to failure by crack opening mode II (by in-plane shearing). Category III contains the new proposed sheet lengthwise compression (SC) tests with free or fixed end conditions. This test was specifically developed for this investigation to determine the OSFFL corresponding to failure by crack opening mode III (by out-of-plane shearing) in sheets. All the tests were carried out at room temperature in an INSTRON Satec 1200 hydraulic testing machine with a constant moving crosshead speed of 2.5 mm/min.

The methods and procedures utilized for determining the FFL and the SFFL are not going to be described in this document because their characterization is explained in a recent publication by Magrinho et al. [7]. For this reason, the following section of the document will be exclusively focused on the determination of the OSFFL (out-of-plane shear fracture forming line) because it will be the first time ever that the failure limit by cracking in mode III is directly obtained from sheets submitted to in-plane compression along one direction.

2.3. Methods and procedures to determine the out-of-plane fracture forming line

The characterization of the OSFFL was performed in rectangular sheet specimens subjected to lengthwise compression with free or fixed ends along its narrower sides (Fig. 4).
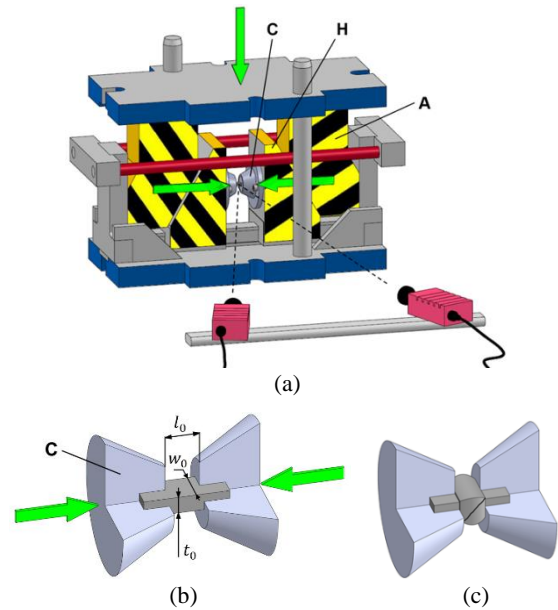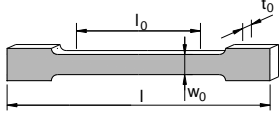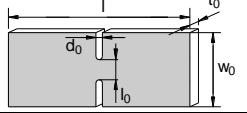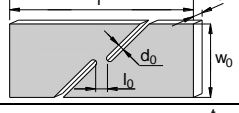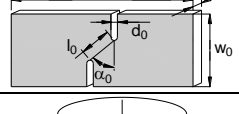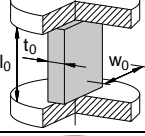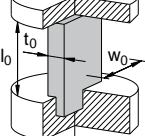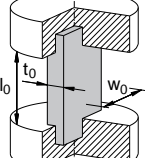

(a)

(b)   (c)

Fig. 4 - Sheet lengthwise compression test: schematic representations of the (a) experimental setup and of the left and right elements of the compression system (b) before and (c) after fracture.

Table 2 - Fracture tests performed in the supplied aluminium AW7075-T651 sheets.

Cat.	Test	l_0 (mm)	w_0 (mm)	t_0 (mm)	l (mm)	d_0 (mm)	α_{RD} (°)	α_0 (°)
I	Tensile test - T	50	12.5	5	200	-	0, 45, 90	-
I	Double notched tensile test - DNT	10, 15	50	5	150	3	0	-
II	Shear test - S	4.72	38.10	5	200	1.63	0	-
II	Staggered double notched tensile test – SDNT	7	50	5	200	3	0	80
III	Sheet lengthwise compression test with free ends – SCF	15	10, 20	5	-	-	0	-
III	Sheet lengthwise compression test with free and fixed ends – SCFC	15	10	5	-	-	0	-
III	Sheet lengthwise compression test with fixed ends – SCC	15	10	5	-	-	0	-

The tests were carried out in a special purpose experimental apparatus that is schematically shown in Fig. 4a. The apparatus consists of a die set with a double-sided compression system. The die set with press-fitted guided pillars contains two compact cam slide units that convert the vertical movement of the actuators (A) into a horizontal movement of the holders (H) towards each other. The holders (H) contain the left and right elements of the compression system (C), which may or may not include clamping features to fix the ends of the specimens (Fig. 4b and 4c). The compression system applies lengthwise forces in both side ends $w_0 \times t_0$ of the specimens and was designed to ensure self-alignment with respect to the vertical centre line. This is crucial to measure the evolution of the in-plane strains at the sheet thickness where cracks are triggered by means of digital image correlation. For this purpose, the specimen thicknesses were sprayed with a stochastic black speckle pattern on a uniform background previously painted in white.

The digital image correlation (DIC) system utilized in the experiments is from Dantec Dynamics, model Q-400 3D, and is equipped with one spotlight and two cameras with 6 megapixels of resolution and 50.2 mm of focal lenses with an aperture of f/11 (Fig. 4a). The frequency of image acquisition was set to 5 frames per second and the correlation algorithm was performed with the INSTRA 4D software. A facet size of 15 pixels with a spacing grid of 5 pixels was employed.

Typical experimental evolutions of the in-plane major ε_1 and minor ε_2 strains obtained from DIC (hereafter designated as the 'experimental strain loading paths') in principal strain space showed a monotonic growth up to the values corresponding to the onset of fracture. The strain loading paths and the fracture strains are plotted in Fig. 5a as solid lines and black solid markers, respectively. The measurements were carried out in the regions where cracks will be triggered, and because the propagation of cracks is instantaneous and accompanied by a sudden relief of stresses it is impossible for the DIC system to continue tracing and comparing digital photographs acquired after cracking.
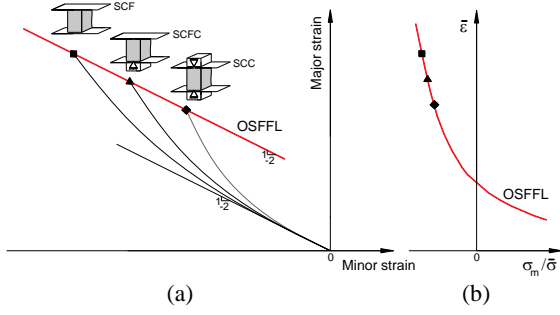
Fig. 5 - Digital image correlation-based methodology for obtaining the strain loading paths and the out-of-plane shear fracture forming line (OSFFL) from sheet lengthwise compression tests: schematic presentations of results in (a) principal strain space and in (b) the space of effective strain vs. stress triaxiality.

The different black solid markers of Fig. 5a correspond to fracture strains of sheet lengthwise compression tests that were carried out with different constrained end conditions. The red straight line with a theoretical slope '-1/2' passing through these markers is the OSFFL (i.e. the fracture locus associated to crack opening by out-of-plane shearing – mode III) [5].

Transformation of the OSFFL from principal strain space to the space of effective strain vs. stress triaxiality (Fig. 5b) requires determining the effective strain $\bar{\varepsilon}$, average stress σ_m and effective stress $\bar{\sigma}$ for all the solid markers corresponding to the experimental values of strain at fracture.

The procedure utilized by the author assumed plastic deformation in the sheet lengthwise compression test to be carried out under proportional loading conditions with a constant ratio β defined as,

$$\beta = \frac{d\varepsilon_2}{d\varepsilon_1} = \frac{\varepsilon_2}{\varepsilon_1} \qquad (3)$$

Considering the application of Hill's 48 yield plasticity criterion [17] under rotational symmetry anisotropy ($\Delta r \cong 0$) and taking into consideration that cracks are triggered at the free surfaces of the specimens experiencing plane stress loading conditions $\sigma_3 = 0$, the effective strain at fracture $\bar{\varepsilon}_f$ is written as,

$$\bar{\varepsilon}_f = \frac{1 + \bar{r}}{\sqrt{(1 + 2\bar{r})}} \sqrt{\varepsilon_{1f}^2 + \varepsilon_{2f}^2 + \frac{2\bar{r}}{(1 + \bar{r})} \varepsilon_{1f}\varepsilon_{2f}} \qquad (4)$$

In the above equation, $(\varepsilon_{1f}, \varepsilon_{2f})$ are the experimental in-plane strain values at fracture retrieved from the solid markers included in Fig. 5a and $\bar{r}$ is the normal anisotropy. The subscript f denotes fracture.

Obtaining the corresponding values of stress triaxiality $\frac{\sigma_m}{\bar{\sigma}}$ requires first writing the effective stress $\bar{\sigma}$, as follows,

$$\bar{\sigma} = \sqrt{\sigma_1^2 + \sigma_2^2 - \frac{2r}{(1 + \bar{r})} \sigma_1\sigma_2} \qquad (5)$$

and then applying the Hill's constitutive equations to establish the following relation between stress triaxiality $\frac{\sigma_m}{\bar{\sigma}}$ and the ratio β of the strain loading path,

$$\frac{\sigma_m}{\bar{\sigma}} = \frac{\sqrt{1 + 2\bar{r}}}{3} \frac{(1 + \beta)}{\sqrt{1 + \frac{2\bar{r}}{(1 + \bar{r})}\beta + \beta^2}} \qquad (6)$$

The above equations (4) and (6) allow transforming the OSFFL from principal strain space to the space of effective strain vs. stress triaxiality (Fig. 5b), as will be required later in the section entitled 'Results and Discussion'.

3. FINITE ELEMENT METHOD

3.1. Modelling conditions

Because the innovative contribution of this document is centered on the sheet lengthwise compression test and crack opening in mode III, it was decided to focus finite element analysis on the numerical simulation of this test with different aspect ratios $\frac{w_0}{l_0}$ and end constraint conditions. The simulations were carried out with the in-house computer program *i-form 3d* that is built upon the rigid-plastic Markov's principle of minimum plastic work modified to include material incompressibility and contact between deformable bodies as additional constrains,

$$\Pi = \int_V \bar{\sigma}\dot{\bar{\varepsilon}}dV + \frac{1}{2}K\int_V \dot{\varepsilon}_v^2 dV - \int_{S_t} T_i u_i dS +$$
$$+ \int_{S_f}\left(\int_0^{|u_r|} \tau_f du_r\right)dS + \qquad (7)$$
$$+ \frac{1}{2}K_1\sum_{c=1}^{N_c}(g_n^c)^2 + \frac{1}{2}K_2\sum_{c=1}^{N_c}(g_t^c)^2$$

In the first three terms of the functional Π, $\bar{\sigma}$ is the effective stress, $\dot{\bar{\varepsilon}}$ is the effective strain rate, $\dot{\varepsilon}_v$ is the volumetric strain rate, K denotes a large positive number that is needed to impose the incompressibility in volume V, T_i and u_i correspond to the surface tractions and velocities on surfaces S_t.

The fourth term accounts for friction along the contact interface S_f between the specimens and the compression system (Fig. 4), where τ_f and u_r are the friction shear stress and the relative sliding velocity between the surfaces. The components of the compression system are modelled as rigid bodies whereas the friction shear stress is modelled by the law of constant friction $\tau_f = mk$ where the friction factor $m = 0.1$ was chosen after checking the finite element predicted forces that best matched the experimental results.

The last two terms are related with self-contact between the plastically deformed surfaces of the test specimens (if existing). For this purpose, the self-contacting surfaces of the specimens are modelled as deformable bodies defined by means of N_c pairs extracted from the sides of the elements that

were utilized in their discretization. The symbols g_n^c and g_t^c denote the normal and tangential gap velocities in the contact pairs, which are penalized by large numbers K_1 and K_2 to avoid penetration.

Fig. 6a shows the initial and final computed meshes retrieved from the numerical simulation of a sheet lengthwise compression test with free ends. Fig. 6b shows a comparison between the finite element predicted and experimental force vs. displacement evolutions. The finite element model made use of symmetry conditions and discretized the test specimen by means of approximately 48000 hexahedral elements. The components of the compression system were discretized by means of contact-friction spatial linear triangular elements.
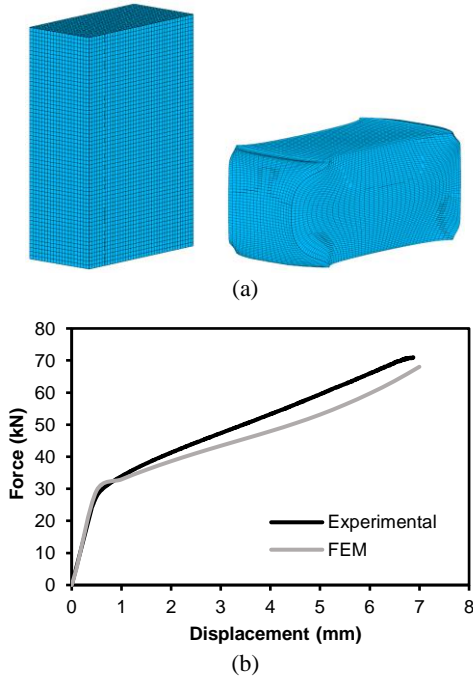

(a)

(b)

Fig. 6 - Finite element simulation of the sheet lengthwise compression test with free ends (SCF, $w_0=10$): (a) Initial and final computed meshes; (b) Comparison between the finite element predicted and experimental evolution of the force with displacement.

3.2. New uncoupled ductile damage criterion

A damage criterion evaluates the plastic deformation accumulation until critical fracture values. There are several criteria and their application depend on the material loading conditions. For crack opening by mode I of fracture mechanics (by tension) (Fig. 7a), the McClintock criterion is commonly used,

$$D_{crit}^I = \int_0^{\bar{\varepsilon}} \frac{\sigma_m}{\bar{\sigma}} d\bar{\varepsilon} \qquad (8)$$

More recently, Christiansen et al. [18] followed an approach to model fracture in shear bands based on opening and growth of neighboring voids by in-plane shear stresses τ (Fig. 7b).
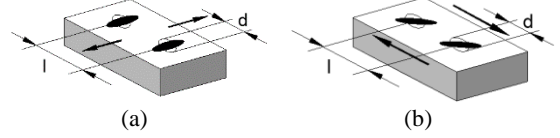

(a)   (b)

Fig. 7 - Schematic representation of void growth in cracking by (a) tension and (b) in-plane shearing.

The starting point of their approach was the work of McClintock et al. [14] on the relationship between the ratio of inter-void spacing l to void diameter d and the average stress σ_m, shear strain γ and strain hardening exponent n,

$$ln\left(\frac{l}{d}\right) =$$
$$ln\sqrt{1+\gamma^2} + \frac{\gamma}{2(1-n)} sinh\frac{(1-n)\sigma_m}{\tau} \qquad (9)$$

Passing the above expression to the integral form as well as approximating the first term on the right side of the equation by $ln\sqrt{1+\gamma^2} \cong \frac{\gamma}{3}$, for shear strains $\gamma < 2$, and simplifying the second term $sinh\left(\frac{(1-n)\sigma_m}{\tau}\right) \approx \frac{(1-n)\sigma_m}{\tau}$ for values of the average and shear stresses of the same order of magnitude,

$$ln\left(\frac{l}{d}\right) \approx \int_0^\gamma \frac{1}{3} d\gamma + \int_0^\gamma \frac{\sigma_m}{2\tau} d\gamma \qquad (10)$$

This allowed Christiansen et al. [18] to derive the following uncoupled ductile damage criterion for crack opening by in-plane shearing in which opening and growth of voids are caused by distortional and dilatational effects,

$$D_{crit}^{II} = \int_0^\gamma \frac{\tau}{\bar{\sigma}} d\gamma + \int_0^\gamma \frac{3}{2} \frac{\sigma_m}{\bar{\sigma}} d\gamma \qquad (11)$$

The first right hand side term of D_{crit}^{II} is the normalized accumulation of plastic shear work per unit of volume $\int \tau d\gamma$ and the second right hand side term introduces the influence of stress triaxiality $\sigma_m/\bar{\sigma}$ in crack opening by in-plane shearing.

One objective of this document is to generalize the ductile damage model proposed by Christiansen et al. [18] to the opening and growth of three-dimensional voids by out-of-plane shearing. For this purpose, considering a general case in which three normal shear stresses and three distortions act simultaneously, ductile damage may be seen as a normalized measure of energy accumulation per unit of volume, given by,

$$D^{III} = \int_0^{\gamma_{ij}} \frac{\tau_{ij}}{\bar{\sigma}} d\gamma_{ij} + \int_0^{\gamma_{ij}} \frac{3}{2} \frac{\sigma_m}{\bar{\sigma}} d\gamma_{ij}$$
$$i,j = 1,3 \quad i \neq j \qquad (12)$$

The critical value of ductile damage D_{crit}^{III} should be obtained from the material shear strain conditions at fracture. Its numerical implementation should not account for the accumulation of negative damage due to dilatational changes when $\sigma_m < 0$ because the closing up of voids under hydrostatic compression in

cold forming does not ensure material healing and recovery of strength.

4. RESULTS AND DISCUSSION

4.1. Fracture in Mode I and Mode II

The fracture forming limits by tension (FFL) and by in-plane shear (SFFL) were determined by means of the experimental tests included in categories I and II of Table 2. Because the methods and procedures utilized in the determination of both fracture limits are comprehensively explained in a recent publication by Magrinho et al. [7], the overall relevance of this first set of results is related to its combination with the ones that will be determined in the following section of the document ('Fracture in mode III').

Still, it is worth presenting the experimental strain loading paths and fracture strains that lead to the determination of the fracture forming limits by crack opening in modes I and II. This is shown in Fig. 8a and the results were achieved by means of the methodology proposed by Magrinho et al. [7], which combines digital image correlation (DIC) and thickness measurements to obtain the 'gauge length' strains at fracture.

As seen in the figure, the FFL is a straight line running from left to right in a downward direction with slope of -1.02 and in good agreement with the theoretical estimate of '-1' [5]. The SFFL is another straight line running from left to right approximately perpendicularly to the FFL [5] and passing through the experimental fracture strain values associated to crack opening in mode II.

The plastic deformation region of the two test specimens selected from categories I and II (Table 2) is revealed in Fig. 8b, in which it is also possible to observe the experimental distributions of the major (top) and minor (bottom) strains immediately before cracking. The end points of the strain loading paths of Fig. 8a were obtained from these strain distributions, or from similar results acquired for other test specimens. The major 'gauge length' strains at fracture ε_{1f} were calculated from,

$$\varepsilon_{1f} = -(\varepsilon_{2f} + \varepsilon_{3f}) \tag{13}$$

where ε_{3f} were obtained from thickness measurements before deformation and after cracking in an optical microscope Mitutoyo TM-505B. The 'gauge length' strain ε_{2f} were taken from the end points of the strain loading paths, assuming localization under plane strain deformation conditions $d\varepsilon_2 = 0$.

Observations in a Hitachi S-2400 scanning electron microscope (SEM) allowed analysing the fractography associated to crack opening modes of the entire set of test specimens that were used in Fig. 8a. The images were obtained with a magnification of 1500x and revealed circular dimples typical of fracture by tension (mode I) in case of the tensile (Fig. 8c) and double notched test specimens.

In what regards the shear (Fig. 8d) and staggered double notched test specimens, the fracture surface consists of elongated parabolic dimpled structures typical of in-plane shearing and compatible with crack opening by mode II.

(a)

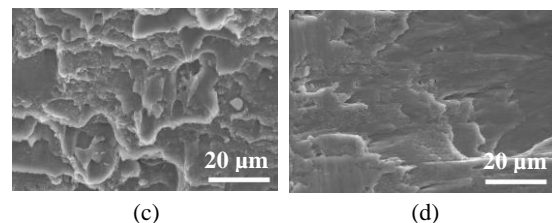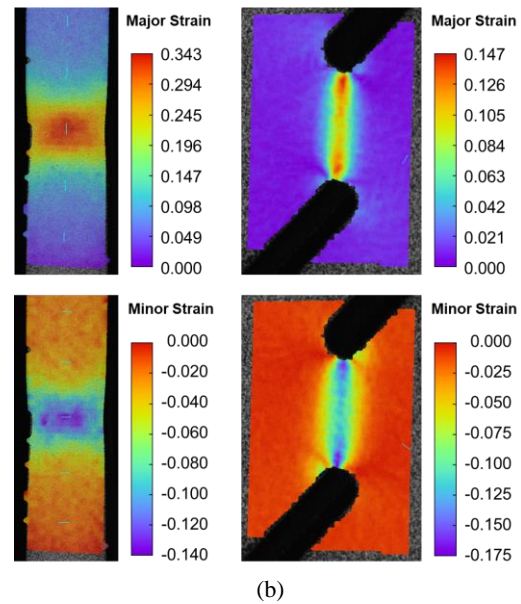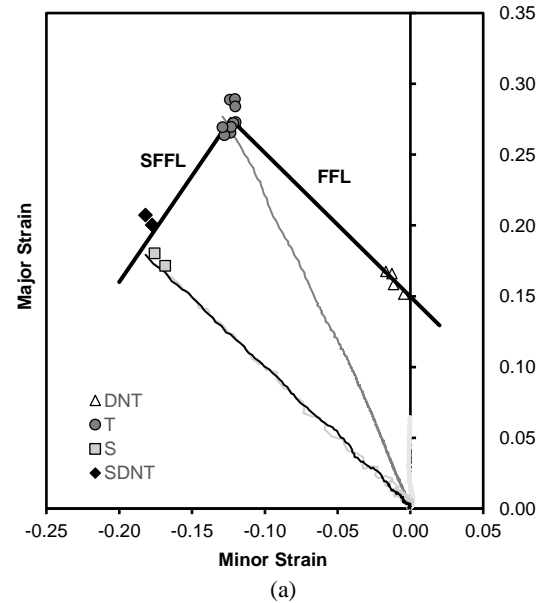(b)

(c)   (d)

Fig. 8 - Fracture forming limits of aluminium AW7075-T651 sheets by tension (FFL) and by in-plane shearing (SFFL): (a) Presentation in principal strain space; (b) Experimental distribution of the major and minor strains at the onset of fracture obtained from DIC for a tensile (left) and a shear (right) test; SEM of the fracture surface of the (c) tensile test specimen and (d) shear test specimen shown in (b);

4.2. Fracture in Mode III

Fig. 9a shows the experimental strain loading paths derived from the sheet lengthwise compression tests with different end support conditions that are listed in Table 2.
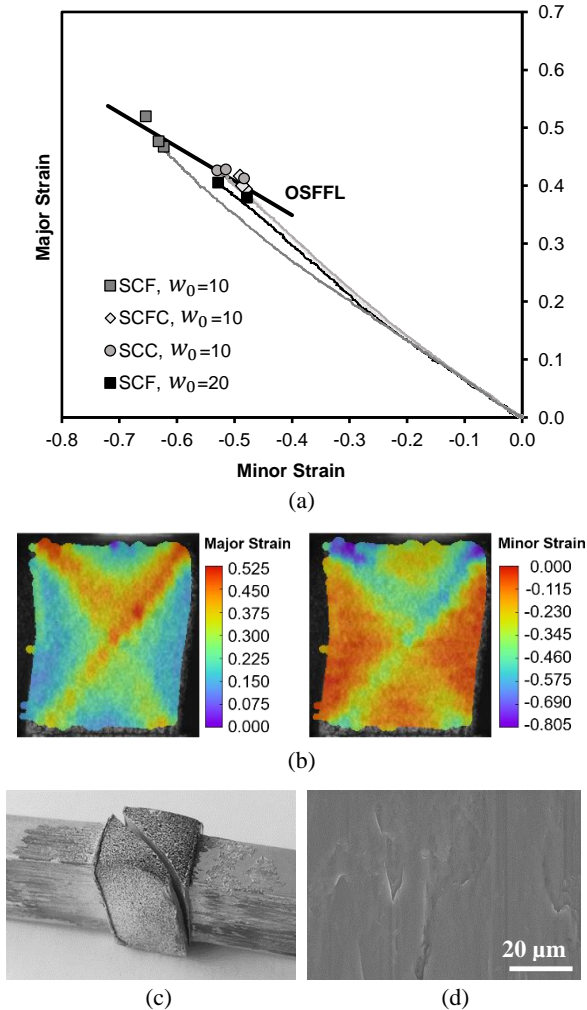

(a)

(b)

(c)

(d)

Fig. 9 - Fracture forming limits of aluminium AW7075-T651 sheets by out-of-plane shearing (OSFFL): (a) Presentation in principal strain space; (b) Experimental distribution of the major (left) and minor (right) strains at fracture for the sheet lengthwise compression tests of a specimen with fixed ends shown in (c); (c) Photograph of sheet lengthwise compression test specimen with fixed ends after cracking; (d) SEM of the fracture surface of the specimens shown in (c).

The experimental setup and the DIC-based methodology to obtain the in-plane major ε_1 and minor ε_2 strains on the thickness surfaces where measurements were performed are described in Section 2.2.

As seen from the photograph included in Fig. 9c, the specimens failed by out-of-plane shearing. The fracture strains were taken from the different end points of the strain loading paths and fall in a straight line running from left to right with a slope of -0.59. This line is the out-of-plane fracture forming limit (OSFFL) and its slope is in good agreement with the theoretical estimate of '-1/2' [5, 19].

Fig. 9b shows the experimental distributions of the major (left) and minor (right) strains obtained by DIC at the instant of time immediately before cracking. The results are provided for a specimen with end-fixed conditions (SCC). The SEM image of the fractured surface is disclosed in Fig. 9d. As seen, the morphology of the fractured surface is smooth and typical of sliding by shearing under pressure. The fractured surface is aligned with the plastic shear band because excessive grain elongation along this surface significantly raises work hardening and eventually promotes the opening and growth of a through-thickness crack (mode III).

Several uncoupled ductile damage criteria were implemented in the finite element computer program *i-form 3d* to predict the exact location where cracks are triggered in sheet lengthwise compression tests. The results are shown in Fig. 10 and allow concluding that the new proposed criterion (refer to Section 3.2) is capable of properly indicating the region of the specimens where cracks are opened – close to the upper and lower corners.

(a)   (b)
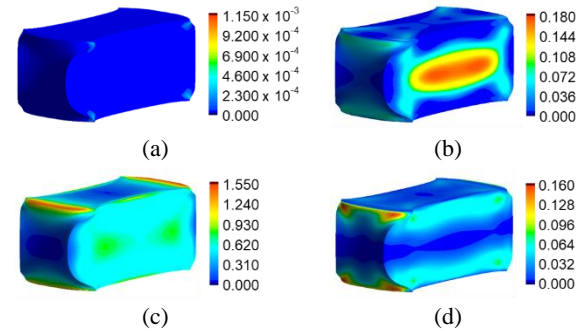
(c)   (d)

Fig. 10 - Finite element predicted distribution of damage for a sheet lengthwise compression test with free ends (SCF) at the instant of deformation where cracks were triggered in the experiments: (a) McClintock criterion (mode I); (b) Normalized Cockroft-Latham criterion; (c) Normalized shear plastic work criterion (mode II); (d) New proposed ductile damage criterion for out-of-plane shearing and failure by mode III.

All the other criteria fail in predicting any accumulation of damage (e.g. McClintock's exclusively based on stress triaxiality [11]), or in providing the correct location of crack initiation (e.g. normalized Cockcroft-Latham and normalized shear plastic work per unit of volume) because they are not appropriate for modelling failure by crack opening in mode III.

4.3. Formability Limits in Sheet-Bulk Forming

This last section of the document starts by merging the fracture forming limits obtained for crack opening by modes I, II and III in principal strain space. The result is shown in Fig. 11a and the fracture loci consists of three distinct limits.

Fig. 11b shows the fracture loci corresponding to the three above mentioned crack opening modes in the space of effective strain vs. stress triaxiality. The transformation of these loci from principal strain

space was carried out by using the methodology described in Section 2.3 and gave once again rise to a two-branch shape distinguishing in-plane from out-of-plane cracking by shearing.
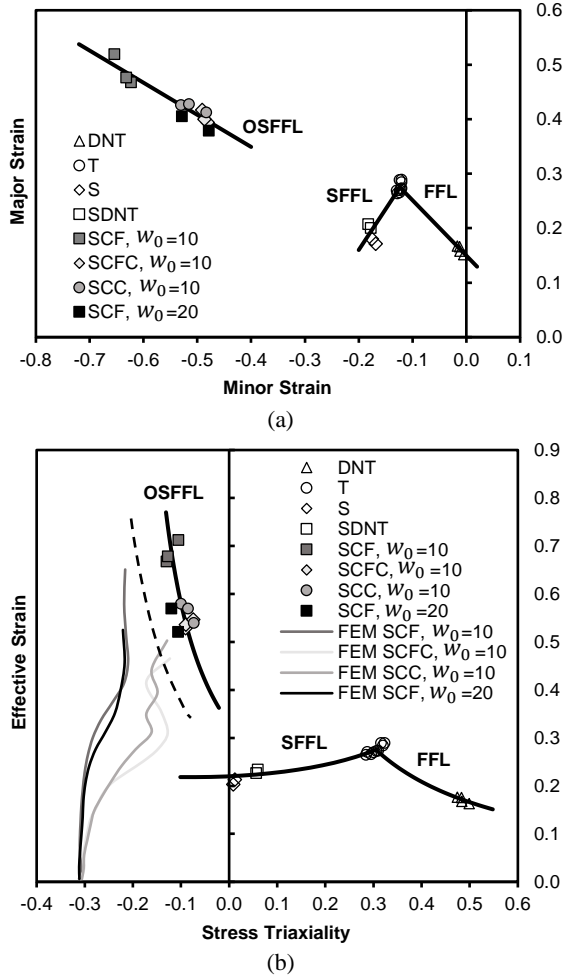

(a)

(b)

Fig. 11 - Fracture forming limits of aluminium AW7075-T651 sheets by tension (FFL), in-plane shearing (SFFL) and out-of-plane shearing (OSFFL): Presentation in (a) principal strain space and in (b) the space of effective strain vs. stress triaxiality.

The finite element computed loading paths of the sheet lengthwise compression tests with different end constraints are plotted as grey curved lines in Fig. 11b. As seen, the loading paths bypass the SFFL on the left side without crossing it, on their way to the OSFFL corresponding to failure by out-of-plane shearing.

The overall agreement between the end points of the finite element computed loading paths and the experimentally determined OSFFL is fair. Major differences are due to the following two reasons. Firstly, the methodology described in Section 2.3 assumes proportional loading with a constant ratio $\beta = \frac{d\varepsilon_2}{d\varepsilon_1} = \frac{\varepsilon_2}{\varepsilon_1}$ whereas the actual loading paths of the sheet lengthwise compression tests shown in Fig. 9a are not linear at the ends. Secondly, the finite element predicted values of effective strain, average strain and effective stress are computed in volume (i.e. per

hexahedral element) instead of being computed on the specimen's surface where measurements were carried out.

The two above-mentioned reasons justify the shift between the OSFFL determined by interpolation of the finite element estimates at the onset of cracking and by the methodology described in Section 2.3 (refer to the dashed and solid OSFFL's included in Fig. 11b).

5. CONCLUSIONS AND FUTURE WORK

Failure by fracture in sheet-bulk forming (SBF) may occur by tension (mode I), in-plane shearing (mode II) and out-of-plane shearing (mode III). The main conclusions derived from the present investigation are the following:

- The new sheet lengthwise compression test that fails by crack opening in mode III can be successfully utilized to determine the fracture forming limit by out-of-plane shearing (OSFFL), for the first time directly from sheets;
- It is difficult, or even impossible, to merge the three different fracture forming limits into a single-branched fracture locus covering the plane stress deformation conditions and the three-dimensional states of stress that are commonly found in SBF;
- Fracture tests must be grouped into three distinct categories depending on the crack opening mode and independently applied to determine the fracture forming limit for each of these categories;
- The proposed experimental-based methodology to transform the fracture loci from principal strain space into the space of effective strain vs. stress triaxiality can be successfully utilized in sheet-bulk forming by using fracture tests that experience proportional or near proportional strain loading paths;
- The new uncoupled ductile damage criterion can be utilized to predict the location where cracks will be triggered by out-of-plane shearing. The criterion was successfully used in the finite element modelling of sheet lengthwise compression tests.

For future work, there are several things that could be interesting to do:

- Repeat the sheet lengthwise compression tests with a more ductile material, where the fracture occurs progressively, to allow the identification of the crack starting point by the digital image correlation system;
- Understand if the fracture would always continue to occur on the specimen-thickness face for a different material;
- Use of new specimen geometries to understand if a greater dispersion of the fracture points would be possible, as well as the union or closer approximation of the OSFFL to the fracture formability limits of modes I and II. It would also

serve to validate the results obtained in this investigation, since the formability limits are a material property, not depending on the specimen geometries;

- Use the sheet lengthwise compression tests with a new design to determine the fracture toughness in mode III;
- Apply the new criterion of damage to other test specimens or parts related to sheet-bulk forming processes to prove the suitability of this criterion.

6. REFERENCES

[1] Merklein, M., Allwood, J.M., Behrens, B.A., Brosius, A., Hagenah, H., Kuzman, K., Mori, K., Tekkaya, A.E., Weckenmann, A. (2012). Bulk forming of sheet metal, CIRP Annals - Manufacturing Technology, 61, pp. 725-745.

[2] Mori, K., Nakano, T. (2016). State-of-the-art of plate forging in Japan, Production Engineering, 10, pp. 81-91.

[3] Lubliner, J. (1990). Plasticity Theory. Macmillan, New York, USA.

[4] Wriggers, P., Simo, J.C., Taylor, R.L. (1985). Penalty and augmented lagrangian formulations for contact problems. In: Proceedings of the NUMETA Conference, Swansea, 97-105.

[5] Martins, P.A.F., Bay, N., Tekkaya, A.E., Atkins, A.G. (2014). Characterization of fracture loci in metal forming, International Journal of Mechanical Sciences, 83, pp. 112–123.

[6] Isik, K., Wernicke, S., Silva, M.B., Martins, P.A.F., Tekkaya, A.E. (2016). Failure by fracture in sheet-bulk metal forming, Journal of Strain Analysis, 51, pp. 387-394.

[7] Magrinho, J.P., Silva, M.B., Reis, L., Martins, P.A.F. (2019). Formability limits, fractography and fracture toughness in sheet metal forming, Materials, 12, pp. 1493.

[8] Erman, E., Kuhn, H.A., Fitzsimons, G. (1983). Novel test specimens for workability testing. In: Compression Testing of Homogeneous Materials and Composites ASTM STP 808. ASTM International, Baltimore, USA, pp. 279.

[9] Magrinho, J.P., Silva, M.B., Alves, L.M., Atkins, A.G., Martins P.A.F. (2018). New methodology for the characterization of failure by fracture in bulk forming, Journal of Strain Analysis, 53, pp 242–247.

[10] Atkins, A.G. (2018). The importance of toughness in manufacturing. Journal of Materials Processing Technology, 261, pp. 280-294.

[11] McClintock, F.A. (1968). A criterion for ductile fracture by the growth of holes, Journal of Applied Mechanics - Transactions of ASME, 35, pp. 363–371.

[12] Ayada, M., Higashino, T., Mori, K. (1987). Central bursting in extrusion of inhomogeneous materials. In: ICTP 1987 - Proceedings of the 2nd International Conference on Technology of Plasticity, Stuttgart, Germany, 1, pp. 553–558.

[13] Cockcroft, M.G., Latham, D.J. (1968). Ductility and the workability of metals, Journal Institute of Metals, 96, pp. 33-39.

[14] McClintock, F.A., Kaplan, S.M., Berg, C.A. (1966). Ductile fracture by hole growth in shear bands, International Journal of Fracture Mechanics, 2, pp. 614-627.

[15] ASTM E8/E8M (2013). Standard Test Methods for Tension Testing of Metallic Materials. ASTM International, West Conshohocken, USA.

[16] ASTM E9 (2018). Standard Test Methods of Compression Testing of Metallic Materials at Room Temperature. ASTM International, West Conshohocken, USA.

[17] Hill, R. (1948). A theory of yielding and plastic flow of anisotropic metals. Proceedings Royal Society London Series A, 193, pp. 281-297.

[18] Christiansen, P., Nielsen, C.V., Bay, N., Martins, P.A.F. (2019). Internal shear cracking in bulk metal forming, Journal of Materials: Design and Applications, 233, pp. 603-614.

[19] Silva, C.M.A., Alves, L.M., Nielsen, C.V., Atkins, A.G., Martins, P.A.F. (2015). Failure by fracture in bulk metal forming, Journal of Materials Processing Technology, 215, pp. 287-298.